Electronic Supplementary Material (ESI) for Journal of Materials Chemistry A.

Supporting Information for

Establishing Upper Bounds on CO_2 Swing Capacity in Sub-Ambient Pressure Swing Adsorption *via* Molecular Simulation of Metal-Organic Frameworks

Jongwoo Park, Ryan P. Lively and David S. Sholl*

School of Chemical & Biomolecular Engineering,
Georgia Institute of Technology, Atlanta, GA 30332 USA

* Corresponding author. E-mail: david.sholl@chbe.gatech.edu.

Table of Contents

S1. Molecular Simulation Details

Atomistic classical GCMC simulations of single component CO_2 adsorption and desorption, and adsorption of a binary CO_2/N_2 0.14/0.86 mixture were conducted on the energy optimized CoRE MOF DDEC charge database using RASPA[1]. Fugacity was converted from pressure using the Peng-Robinson equation of state.[1] All the MOF structures investigated are approximated by rigid model with triclinic boundary conditions employeed in all dimensions. A rigid and linear model was used for both CO_2 and N_2 molecules. Lennard-Jones parameters for framework atoms are obtained from the UFF[2] which is widely used force field for MOFs, and the parameters for CO_2 and N_2 are obtained from the TraPPE[3] force field. In Monte Carlo simulation associated with these force fields, the truncated potentials with tail corrections are applied. Simulation volumes are expanded to at least 26 Å along each dimension and LJ interactions are truncated at 12 Å. Electrostatic interactions were computed pairwise with a long range Ewald summation scheme[4] based on atomic point charges assigned *via* DDEC method. DDEC is one of multiple methods to assign electrostatic charges to framework atoms, and it is based on the electron density partitioning in periodic structures.[5] The point charges are found by minimizing an optimization functional to reproduce both the charge distribution and local electrostatic potential.[5]

All GCMC calculations included 5,000 initialization cycles to equilibrate the positions of the atoms in the system followed by 50,000 production cycles. A Monte Carlo cycle consists of N steps where N is the number of molecules in the system. Random Monte Carlo moves, either accepted or rejected according to Boltzmann-type weighting criteria, allowed translation, rotation, regrowth, reinsertion, deletion and insertion moves at the identical probabilities. For a mixture gas adsorption simulation, a Monte Carlo move that swapped the identity of existing molecules associated with the competitive adsorption of each component was imposed in addition to above random Monte Carlo moves.

Isosteric heats of adsorption (Q_{ads}) was computed during GCMC simulations based on the fluctuation method.[1] The heat of adsorption at zero loading (Q_{ads}^{0}) was also computed in the canonical ensemble.[6,7] Q_{ads}^{0} is an indicator for the host-adsorbate affinity under infinite dilute conditions.[6] Random Monte Carlo moves in this simulation allowed translation, rotation, regrowth, and reinsertion moves at the identical probabilities.

The void fraction of each computation-ready structure was calculated from a Widom particle insertion method using a He probe molecule (ε/k_B = 10.9 K, σ = 2.64 Å) at 298 K.[1] The pore volume was calculated by multiplying the void fraction with the unit cell volume. The accessible surface area was calculated by using N_2 as probe molecule with overlap distance criteria set to a size parameter σ of 3.31 Å.[1] The largest cavity diameter and the pore limiting diameter were calculated by Zeo++ applying the high-accuracy setting with a probe of radius 1.86 Å, corresponding to N_2.[8]

S2. Sub-Ambient PSA CO_2 Swing Capacity in MOFs

S2.1. Geometric Properties of MOFs for Swing Capacity

The pore volume (V_P) is one of the most critical geometric properties that governs physisorption of adsorbate molecules. There are also other geometric indicators that could potentially be used to estimate CO_2 capture performance using porous materials. They include the accessible surface area (SA_{acc}), largest cavity diameter (LCD), and the pore limiting diameter (PLD). Here we examine correlations between each property and sub-ambient PSA CO_2 swing capacity.

Fig. S1 shows the correlation between V_P and swing capacity at 228 K and 243 K. The existence of materials with large swing capacities of 25 - 35 mol/kg at 228 K and 18 - 23 mol/kg at 243 K are observed. As discussed, the correlation between V_P and swing capacity becomes more pronounced at lower temperature.

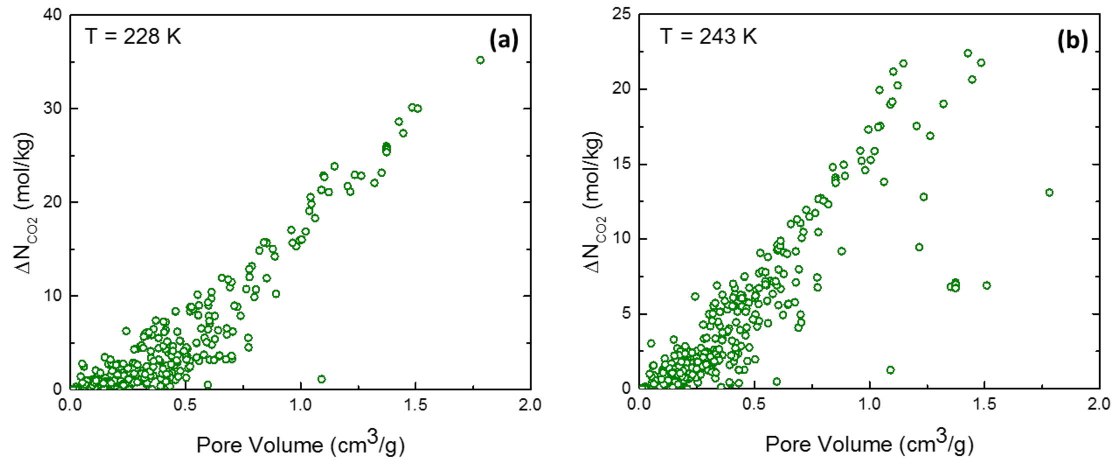

Fig. S1. Calculated CO_2 swing capacity between 0.1 bar and 2.0 bar in 477 MOFs at (a) 228 K and (b) 243 K.

Fig. S2 shows the computed PSA swing capacity as a function of four representative geometric MOF properties at 243 K. Large V_P and SA_{acc} show clear correlations to accomplish high swing capacities. We note that V_P and SA_{acc} are stronlgy correlated to one another. LCD and PLD exhibit poor correlation to achieve large swing capacities. Similar results were seen at other temperatures (data not shown).

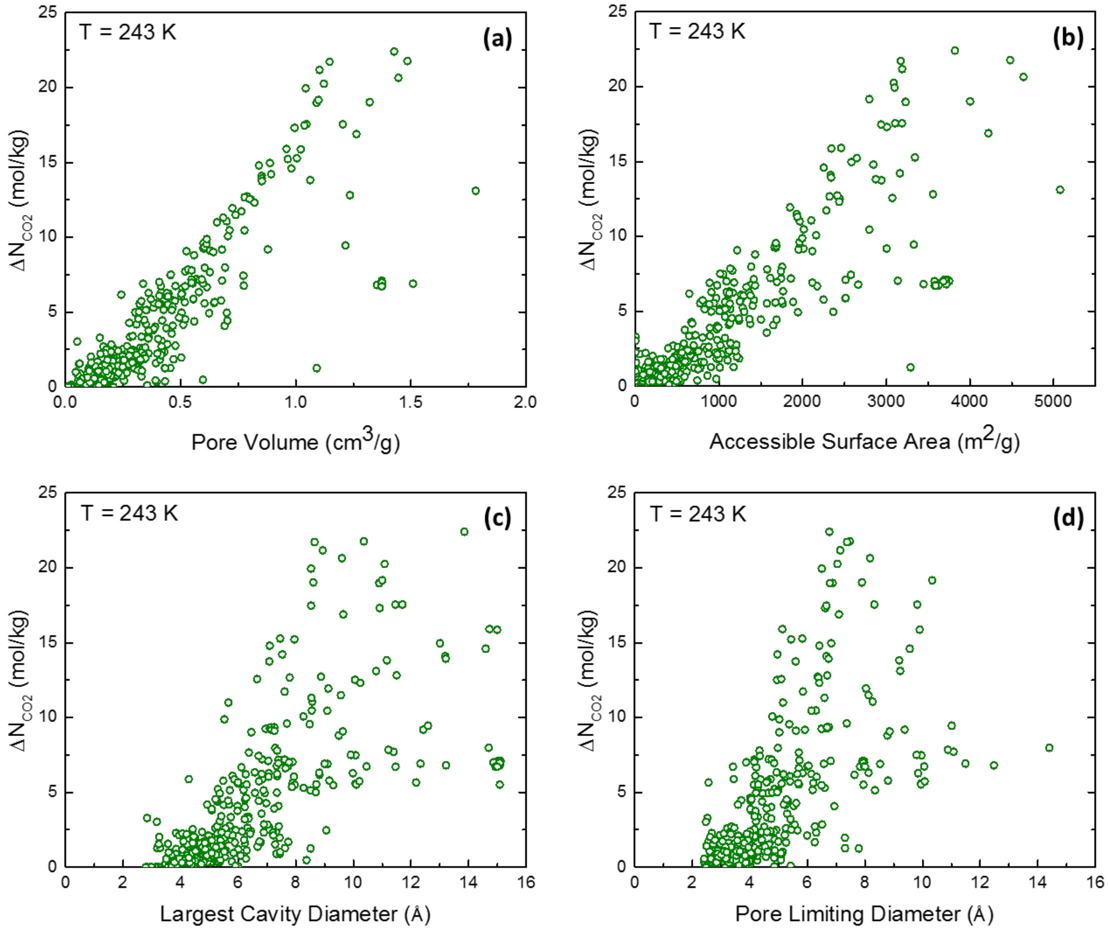

Fig. S2. Calculated CO_2 swing capacity between 0.1 bar and 2.0 bar in 477 MOFs at 243 K as a function of (a) pore volume, (b) accessible surface area, (c) largest cavity diameter, and (d) pore limiting diameter.

S2.2. Energetic Properties of MOFs for Swing Capacity

Once geometric criteria are satisfied, it is useful to observe how energetic properties of MOFs enable large swing capacity as discussed in the manuscript. The predicted sub-ambient PSA CO_2 swing capacity as a function of Q_{ads}^0 and Q_{ads}^{avg} is investigated in Fig. S3a and Fig. S3b, respectively. The presence of the optimal heat range at different temperatures are observed for both quantities. The optimum for both thermodynamic quantities to achieve a breakthrough improvement in a PSA process is weakly temperature dependent. The correlation between Q_{ads}^0 and Q_{ads}^{avg} in Fig. S3c shows that the majority of the materials show the increase in Q_{ads} as loading increases with optimal Q_{ads}^0 and Q_{ads}^{avg} for large swing capacity.

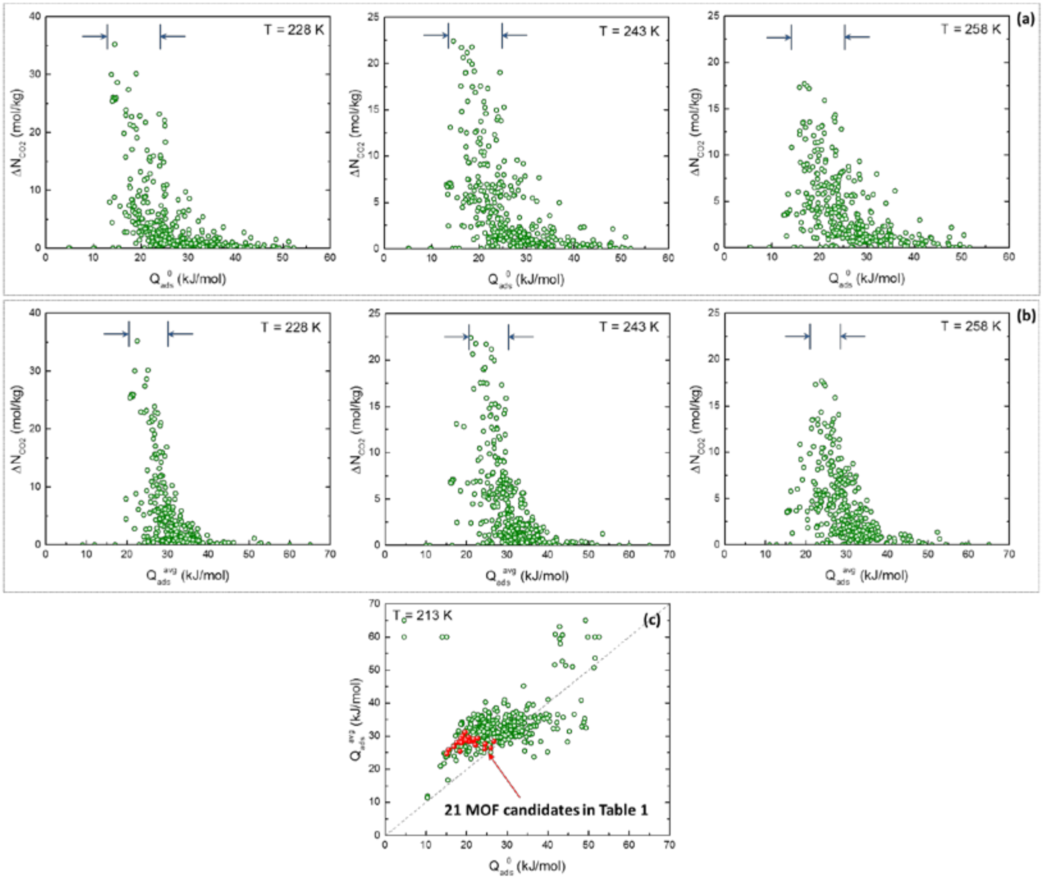

Fig. S3. (a) Q_{ads}^0 and (b) Q_{ads}^{avg} at 228 K, 243 K, and 258 K in 477 MOFs. Arrows indicate the optimal range for the heat of adsorption. (c) Correlation between Q_{ads}^0 and Q_{ads}^{avg} at 213 K in 477 MOFs with entries of high swing capacity 21 MOF candidates noted.

S2.3. MOF Candidates for Large Sub-Ambient PSA CO_2 Swing Capacity

Table S1. MOF candidates for large sub-ambient PSA ΔN_{CO2} with geometric [a] and energetic properties

Metal-Organic Frameworks	V_P (cm^3/g)	SA_{acc} (m^2/g)	LCD (Å)	PLD (Å)	Q_{ads}^0 (kJ/mol)					Q_{ads}^{avg} (kJ/mol)				
					213 K	228 K	243 K	258 K	273 K	213 K	228 K	243 K	258 K	273 K
XAWVUN	1.8	5077	10.8	9.2	15.1	14.5	13.9	13.4	12.9	24.7	22.5	17.5	16.2	15.7
ANUGIA	1.4	3820	13.9	6.8	15.6	15.1	14.6	14.2	13.7	26.0	24.7	21.1	18.5	17.7
WONZOP	1.1	2796	11.0	10.3	20.7	19.8	19.0	18.1	17.3	28.3	26.9	24.5	20.9	19.9
SENWAL	1.2	3171	8.7	7.4	17.5	16.9	16.3	15.8	15.3	28.2	26.7	24.8	22.3	19.7
YUGLES	1.1	3231	10.9	6.8	18.4	17.8	17.1	16.5	15.9	25.5	26.1	24.2	21.5	19.2
NUTQAV	1.1	3229	10.9	6.9	18.4	17.8	17.2	16.6	16.1	28.1	26.0	24.3	21.6	19.4
WONZUV	1.2	3187	11.5	9.8	21.7	21.0	20.3	19.6	19.0	28.5	26.7	23.4	21.8	21.6
OJICUG	1.3	4001	8.6	7.9	25.9	25.0	24.4	23.3	22.6	26.4	26.1	24.1	23.6	23.4
NUTQEZ	1.1	3105	11.7	8.3	16.8	16.5	16.2	15.9	15.5	26.9	26.2	24.1	21.3	19.6
SENWOZ	1.1	3189	8.9	7.1	18.6	18.1	17.5	16.9	16.3	29.3	27.5	26.1	23.8	21.2
MATVEJ	1.0	2938	8.5	6.7	19.9	19.2	18.6	17.9	17.4	28.7	26.8	24.9	22.8	21.1
UTEWUM	1.0	2342	15.0	9.9	21.8	21.4	21.0	20.6	20.2	29.1	29.7	29.7	26.4	23.7
XAMDUM07	0.9	2338	13.2	6.7	24.4	24.1	23.8	23.4	22.9	26.2	26.8	25.8	23.8	22.4
FIQCEN	0.9	2333	13.2	6.7	24.6	24.3	23.9	23.5	23.0	27.6	27.6	26.0	24.2	22.5
UTEWOG	1.0	2251	14.6	9.6	22.2	21.8	21.4	21.0	20.6	27.3	29.3	29.5	26.7	24.1
BIBXUH	1.0	2458	14.7	5.1	18.8	18.1	17.6	17.1	16.6	28.0	26.9	24.8	22.8	21.2
XUGSEY	1.0	3342	7.5	5.8	26.7	26.1	25.2	24.6	23.8	28.4	28.0	27.1	25.2	23.9
KEFBEE	1.1	3088	11.1	7.0	19.0	18.5	17.9	17.4	16.9	30.0	28.2	26.1	24.2	22.1
FEFCUQ	0.8	2413	8.9	6.4	20.5	20.0	19.5	19.0	18.5	29.7	27.9	26.1	23.9	22.3
QUQFIS	1.0	2646	8.0	5.4	22.7	21.9	21.3	20.5	19.8	29.4	27.1	26.1	24.6	22.7
SENWIT	1.0	3098	8.5	6.5	19.6	19.0	18.5	17.8	17.3	31.2	28.1	26.8	24.7	22.5

[a] Geometric properties were adapted from CoRE MOF database developed by Chung *et al.*[9] with some properties recomputed in this work if needed.

S3. Desorption Condition in Sub-Ambient PSA CO_2 Swing Capacity

The choice of desorption pressure in a PSA process strongly affects the energy and cost efficiency of the overall process.[10] The analysis in the manuscript used a desorption pressure of 0.1 bar, which may be considerably lower than is desirable in practice. Here, we examine the influence of the desorption pressure on the CO_2 swing capacities in a number of large capacity MOFs.

Fig. S4 - S6 show the computed CO_2 adsorption isotherms, heat of adsorption, predicted swing capacities by varying desorption pressures from 0.1 to 1.0 bar in ANUGIA (Fig. S4), WONZOP (Fig. S5), and SENWAL (Fig. S6). Two observations can be made from these results. First, all three materials achieve 10 mol/kg swing capacities at 243 and/or 258 K using a pressure swing between 2.0 bar for adsorption and 1.0 bar for desorption. Second, the temperature at which the maximum swing capacity is observed increases as the desorption pressure is increased. This observation, coupled with the reduced swing capacity as the desorption pressure is increased, indicate that a set of tradeoffs will dictate the optimal desorption pressure and operating temperature in designing an optimal PSA process.

Fig. S4 - S6 also show the mixture adsorption selectivity for CO_2 relative to a bulk binary CO_2/N_2 0.14/0.86 mixture in ANUGIA (Fig. S4), WONZOP (Fig. S5), and SENWAL (Fig. S6). As expected, lowering the temperature increases the adsorption selectivity in every example. These materials have higher selectivities than the high capacity material shown in Fig. 6. WONZOP (Fig. S5) and SENWAL (Fig. S6) both show selectivities exceeding 40 at 213 K. All of the materials in Fig. S4 - S6 and Fig. 6 show only moderate selectivity at 258 K and 273 K.

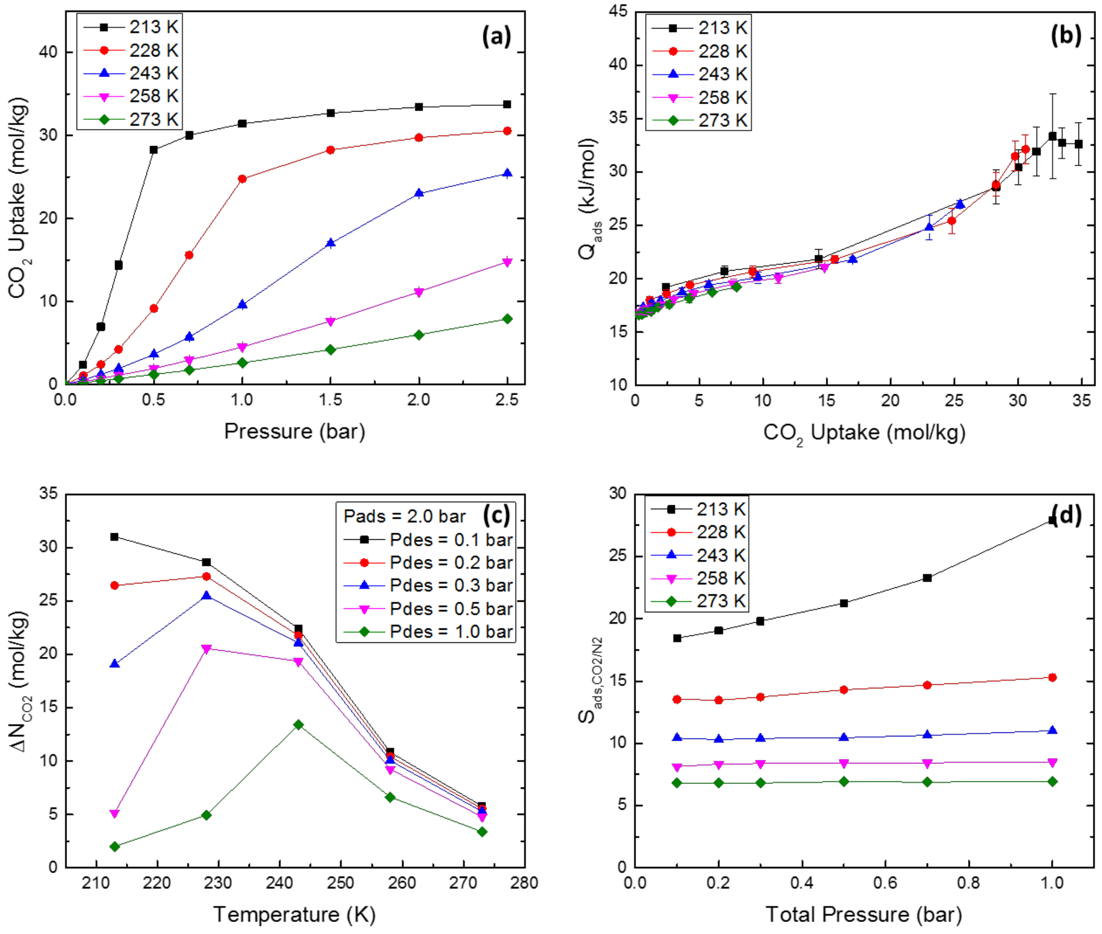

Fig. S4. (a) Sub-ambient CO_2 adsorption isotherms computed by GCMC simulations, (b) heat of adsorption as a function of CO_2 uptake obtained from GCMC simulation, (c) predicted sub-ambient PSA CO_2 swing capacity as a function of desorption pressure, and (d) CO_2 adsorption selectivity from bulk CO_2/N_2 0.14/0.86 mixture calculated by binary GCMC simulations in ANUGIA.

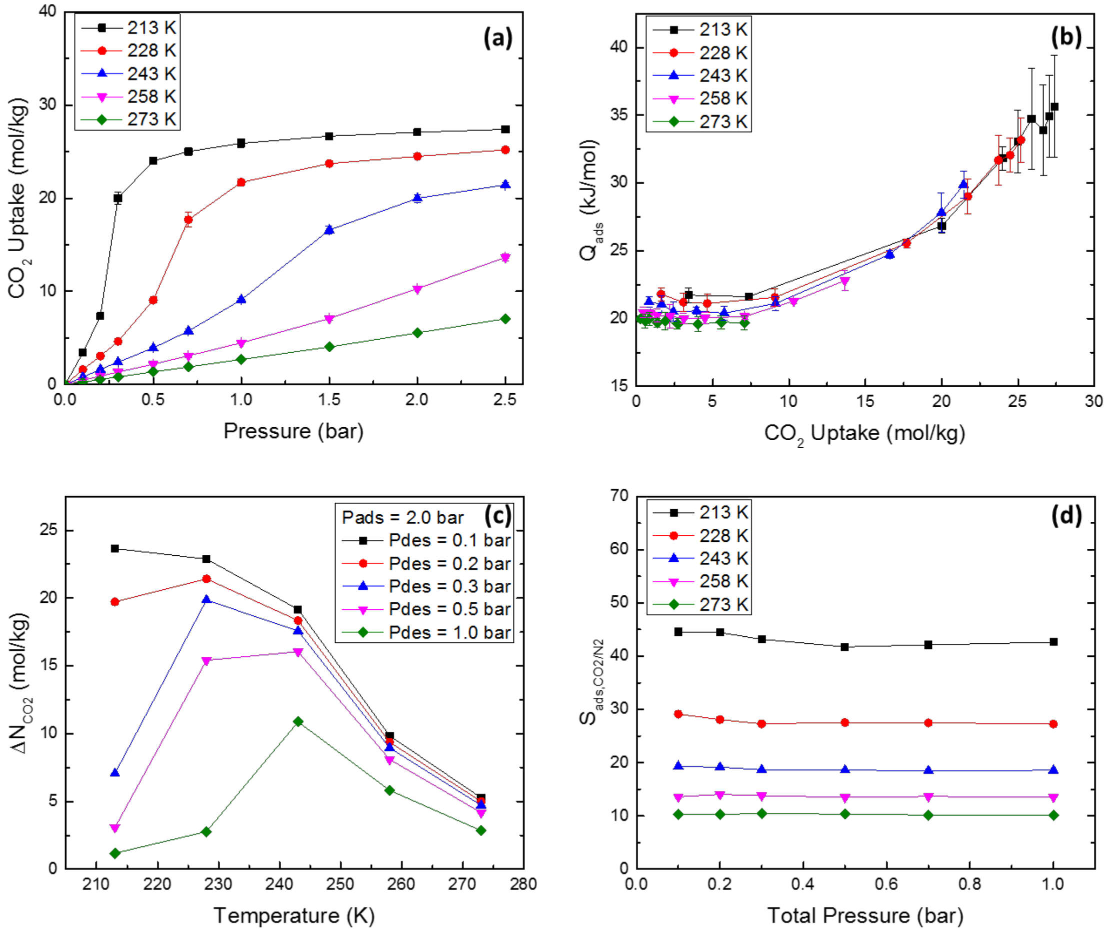

Fig. S5. (a) Sub-ambient CO_2 adsorption isotherms computed by GCMC simulations, (b) heat of adsorption as a function of CO_2 uptake obtained from GCMC simulation, (c) predicted sub-ambient PSA CO_2 swing capacity as a function of desorption pressure, and (d) CO_2 adsorption selectivity from bulk CO_2/N_2 0.14/0.86 mixture calculated by binary GCMC simulations in WONZOP.

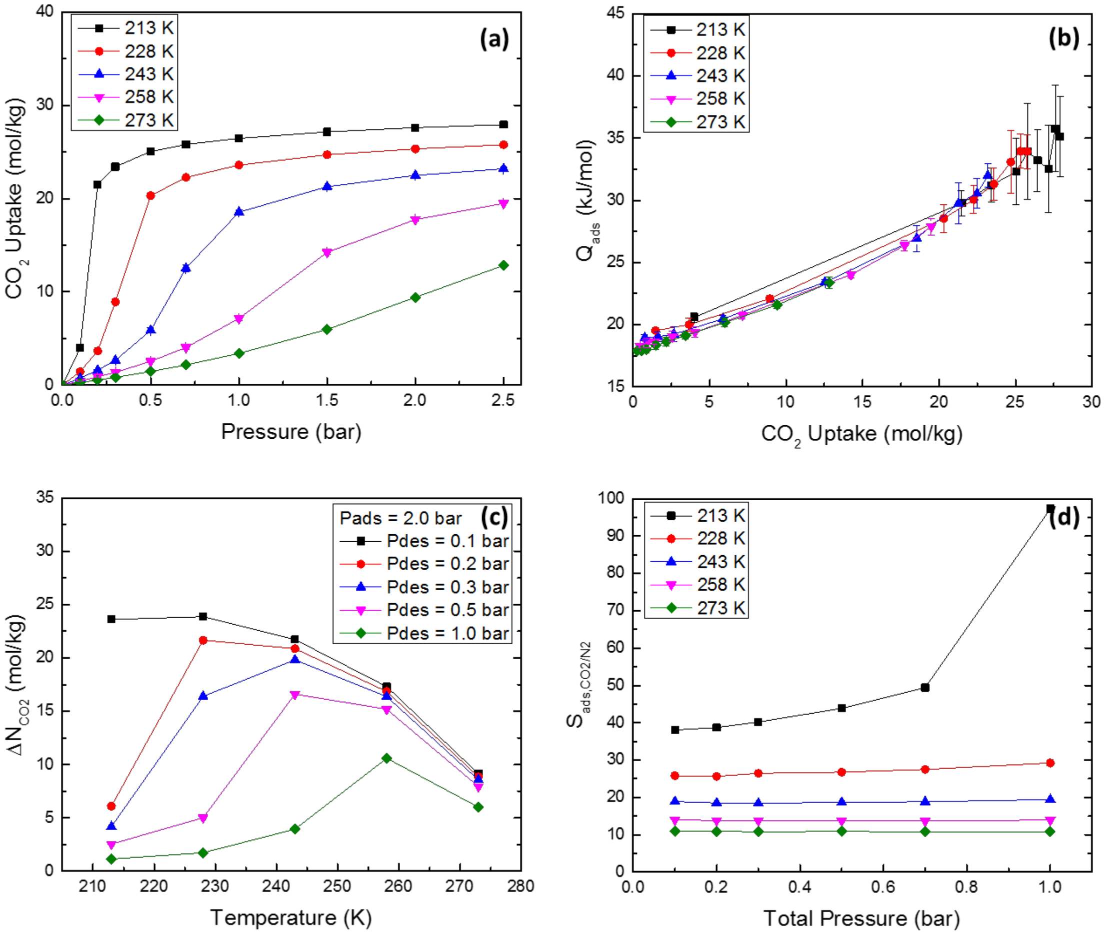

Fig. S6. (a) Sub-ambient CO_2 adsorption isotherms computed by GCMC simulations, (b) heat of adsorption as a function of CO_2 uptake obtained from GCMC simulation, (c) predicted sub-ambient PSA CO_2 swing capacity as a function of desorption pressure, and (d) CO_2 adsorption selectivity from bulk CO_2/N_2 0.14/0.86 mixture calculated by binary GCMC simulations in SENWAL.

References

1 D. Dubbeldam, A. Torres-Knoop and K. S. Walton, *Molecular Simulation*, 2013, **39**, 1253-1292.

2 A. K. Rappe, C. J. Casewit, K. S. Colwell, W. A. Goddard and W. M. Skiff, *Journal of the American Chemical Society*, 1992, **114**, 10024-10035.

3 M. G. Martin and J. I. Siepmann, *Journal of Physical Chemistry B*, 1998, **102**, 2569-2577.

4 B. A. Wells and A. L. Chaffee, *Journal of Chemical Theory and Computation*, 2015, **11**, 3684-3695.

5 T. A. Manz and D. S. Sholl, *Journal of Chemical Theory and Computation*, 2010**, 6**, 2455-2468.

6 D. D. Do, D. Nicholson and H. D. Do, *Journal of Colloid and Interface Science*, 2008, **324**, 15-24.

7 A. N. Dickey, A. O. Yazaydin, R. R. Willis and R. Q. Snurr, *Canadian Journal of Chemical Engineering*, 2012, **90**, 825-832.

8 T. F. Willems, C. Rycroft, M. Kazi, J. C. Meza and M. Haranczyk, *Microporous and Mesoporous Materials*, 2012, **149**, 134-141.

9 Y. G. Chung, J. Camp, M. Haranczyk, B. J. Sikora, W. Bury, V. Krungleviciute, T. Yildirim, O. K. Farha, D. S. Sholl and R. Q. Snurr, *Chemistry of Materials*, 2014, **26**, 6185-6192.

10 M. T. Ho, G. W. Allinson and D. E. Wiley, *Industrial & Engineering Chemistry Research*, 2008, **47**, 1562-1568.